10-25-2022

Novel chelating agents for zirconium-89-positron emission tomography (PET) imaging: Synthesis, DFT calculation, radiolabeling, and in vitro and in vivo complex stability

Chi Soo Kang

Shuyuan Zhang

Haixing Wang

Yujie Liu

Siyuan Ren

See next page for additional authors

Authors

Chi Soo Kang, Shuyuan Zhang, Haixing Wang, Yujie Liu, Siyuan Ren, Yanda Chen, Jingbai Li, Nilantha Bandara, Andrey Yu Rogachev, Buck E Rogers, and Hyun-Soon Chong

ACS OMEGA

http://pubs.acs.org/journal/acsodf

Article

Novel Chelating Agents for Zirconium-89-Positron Emission Tomography (PET) Imaging: Synthesis, DFT Calculation, Radiolabeling, and *In Vitro* and *In Vivo* Complex Stability

Chi Soo Kang, Shuyuan Zhang, Haixing Wang, Yujie Liu, Siyuan Ren, Yanda Chen, Jingbai Li, Nilantha Bandara, Andrey Yu Rogachev, Buck E. Rogers, and Hyun-Soon Chong*

Cite This: *ACS Omega* 2022, 7, 37229−37236

Read Online

ACCESS | Metrics & More | Article Recommendations | Supporting Information

ABSTRACT: We report the synthesis and evaluation of novel chelating agents for zirconium-89 (^{89}Zr) with positron emission tomography (PET) imaging applications. New chelating agents NODHA, NOTHA, and NODHA-PY were constructed on 1,4,7-triazacyclononane (TACN) and possess hydroxamic acid or a pyridine ring as an acyclic binding moiety. The new chelating agents were theoretically studied for complexation with Zr(IV). Structures of Zr(IV)-NODHA, Zr(IV)-NOTHA, and Zr(IV)-NODHA-PY were predicted using density functional methods. NODHA was found to form stronger bonds with Zr(IV) when compared to NOTHA and NODHA-PY. The new chelating agents were evaluated for radiolabeling efficiency in binding ^{89}Zr. The corresponding [^{89}Zr]Zr-labeled chelators were evaluated for complex stability in human serum. All new chelating agents rapidly bound to ^{89}Zr in excellent radiolabeling efficiency at room temperature. Among the new [^{89}Zr]Zr-labeled chelators evaluated, [^{89}Zr]Zr-NODHA showed the highest stability in human serum without losing ^{89}Zr, and [^{89}Zr]Zr-NODHA-PY released a considerable amount of ^{89}Zr in human serum. [^{89}Zr]Zr-NODHA, [^{89}Zr]Zr-NODHA-PY, and [^{89}Zr]Zr-DFO were comparatively evaluated for *in vivo* complex stability by performing biodistribution studies using normal mice. [^{89}Zr]Zr-DFO had the lowest bone uptake at all time points, while [^{89}Zr]Zr-NODHA-PY showed poor stability in mice as evidenced by high bone accumulation at the 24 h time point. [^{89}Zr]Zr-NODHA exhibited better renal clearance but higher bone uptake than [^{89}Zr]Zr-DFO.

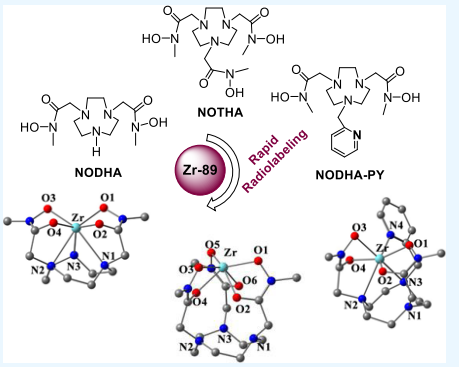

INTRODUCTION

Positron emission tomography (PET) is a clinically available imaging method that employs a radioactive tracer for detection of various diseases including cancer.[1−3] 2-Deoxy-2-[^{18}F]-fluoroglucose ([^{18}F]FDG) is the most frequently used PET tracer in oncology. However, [^{18}F]FDG has clinical limitations including nontarget specificity and short biological half-life.[4] To overcome the limitation of ^{18}F-FDG, the development of monoclonal antibody (mAb)-based PET tracers, which can specifically image tumor sites using the mAb's exquisite specificity and high affinity against antigens, has attracted a lot of attention.[5−7] Accordingly, various positron-emitting radioisotopes including ^{86}Y, ^{64}Cu, and ^{68}Ga have been explored for the development of PET tracers.[8,9] However, the metallic radionuclides have some drawbacks that hamper the optimal construction of antibody-based PET tracers. For instance, ^{64}Cu ($t_{1/2}$ = 12.7 h), ^{68}Ga ($t_{1/2}$ = 67.7 min), and ^{86}Y ($t_{1/2}$ = 14.7 h) have too short half-life for PET applications of antibody with long biological half-life.[8,9] On the other hand, ^{89}Zr has physical properties suitable for antibody-targeted PET imaging applications, and its half-life ($t_{1/2}$ = 78.4 h) is compatible with biological half-life of the typical antibodies.[9,10] The methods for production of ^{89}Zr with high radiochemical purity and specific activity are well developed, although its high energy γ radiation (909 keV) necessitates proper shielding and limits injection dose.[10−12] Recognition of ^{89}Zr as an adequate radioisotope for the application of molecularly targeted PET imaging led to the investigations on the development of appropriate chelators, which is a critical component in PET tracers centered on a metallic radioisotope.[7,13] Since the hydroxamate group has high affinity for zirconium(IV), desferrioxamine (DFO), a siderophore containing three hydroxamate groups, has been extensively explored for the development of PET imaging agents.[14−16] Nevertheless, DFO is not an ideal chelate for targeted PET imaging applications as it has been shown that ^{89}Zr was liberated from the ^{89}Zr complexes of DFO-antibody conjugates and accumulated in bone *in vivo*.[16,17]

Received: June 3, 2022
Accepted: August 19, 2022
Published: October 13, 2022

Scheme 1. Synthesis of Chelators NODHA (5) and NOTHA (6)

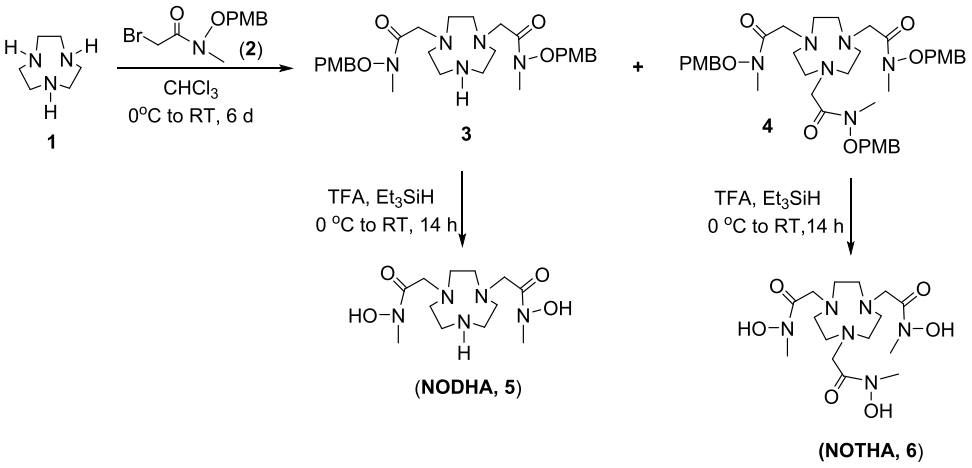

Scheme 2. Synthesis of Compound 3

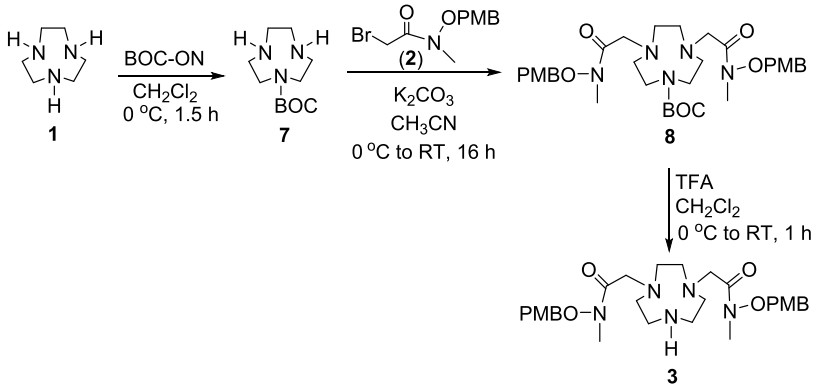

Scheme 3. Synthesis of NODHA-PY (10)

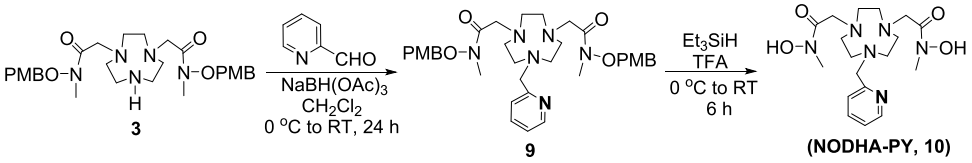

Our continued effort to develop chelation chemistry for radionuclides with broad applications in cancer therapy and imaging has led us to design and synthesize novel chelates for ^{89}Zr. New chelating agents (NODHA, NOTHA, and NODHA-PY) are structured on 1,4,7-triazacyclononane (TACN) and contain hydroxamic acid (HA) or a pyridine (PY) ring as an acyclic binding moiety. The novel chelates were evaluated and compared with the gold standard DFO for their radiolabeling kinetics and complex stability in human serum with ^{89}Zr. In addition, a biodistribution study using normal mice was conducted to investigate *in vivo* stability of [^{89}Zr]Zr-NODHA, [^{89}Zr]Zr-NODHA-PY, and [^{89}Zr]Zr-DFO.

RESULTS AND DISCUSSION

Synthesis. Synthesis of chelators NODHA and NOTHA is outlined in Scheme 1. The reaction of 1,4,7-triazacyclononane (TACN) **1** with compound **2**[18] in $CHCl_3$ afforded both bisubstituted TACN **3** (34% isolated yield) and trisubstituted TACN **4** (16% isolated yield). The *p*-methoxybenzyl (PMB) groups in compounds **3** and **4** were removed using trifluoroacetic acid (TFA) and triethylsilane to produce the desired chelators NODHA (**5**) and NOTHA (**6**)[19] in the respective isolated yield of 81% and 93%. Improved synthesis of the key precursor **3** to NODHA is outlined in Scheme 2. TACN (**1**) was selectively reacted with BOC-ON to obtain *N*-BOC-protected TACN (**7**).[20] The base-promoted reaction of **2** and **7** provided compound **8** in 84% isolated yield. The BOC group in compound **8** was removed by treatment of **8** with TFA to give compound **3** in 96% isolated yield. Synthesis of NODHA-PY containing the pyridine ring is outlined in Scheme 3. Reductive amination of compound **3** with 2-formyl pyridine using sodium triacetoxyborohydride as a reducing agent afforded compound **9**. The PMB groups in **9** were removed by treatment of compound **9** with TFA and triethylsilane to generate the target chelator NODHA-PY (**10**).

Density Functional Theory (DFT) Calculations. We conducted theoretical studies on complexation of the new chelators NODHA (**5**), NOTHA (**6**), and NODHA-PY (**10**) with Zr(IV) using the DFT method (Table 1). NODHA (**5**) is predicted to form a seven-coordinate complex with Zr using all nitrogen and oxygen donors. The oxygen atoms in the DFT-

https://doi.org/10.1021/acsomega.2c03478
ACS Omega 2022, 7, 37229−37236

Table 1. Distance (Å) of Selected Bonds in the DFT-Calculated Structure of Zr(IV)-NOTHA, Zr(IV)-NODHA, and Zr(IV)-NODHA-PY

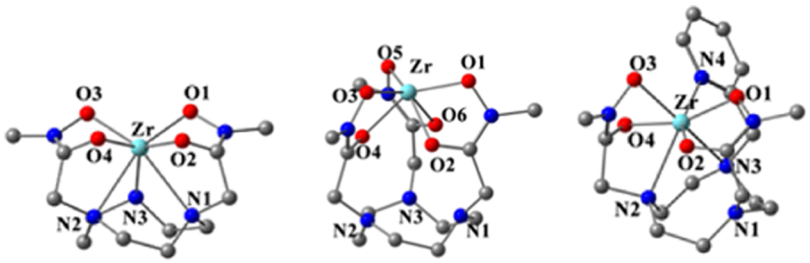

bond distance (Å)	Zr(IV)-NODHA	Zr(IV)-NOTHA	Zr(IV)-NODHA-PY
Zr-O1	2.070	2.066	2.068
Zr-O2	2.050	2.123	2.067
Zr-O3	2.082	2.068	2.080
Zr-O4	2.050	2.121	2.239
Zr-O5		2.069	
Zr-O6		2.122	
Zr-O (mean)	**2.063**	**2.095**	**2.114**
Zr-N1	2.691	4.379	3.469
Zr-N2	2.648	4.373	2.573
Zr-N3	2.401	4.378	2.496
Zr-N4			2.297
Zr-N (mean)	**2.580**	**4.377**	**2.709**

Table 2. Radiolabeling Efficiency (%) of Chelators with ^{89}Zr (n = 2, pH 7.0, RT)[a]

	radiolabeling efficiency (%)			
time	[^{89}Zr]Zr-NODHA	[^{89}Zr]Zr-NOTHA	[^{89}Zr]Zr-NODHA-PY	[^{89}Zr]Zr-DFO
1 min	94.7 ± 0.5	98.4 ± 0.6	95.9 ± 0.6	100.0 ± 0.0
5 min	100.0 ± 0.0	100.0 ± 0.0	97.5 ± 0.8	100.0 ± 0.0
10 min	100.0 ± 0.0	94.7 ± 7.5	97.2 ± 3.9	100.0 ± 0.0
30 min	100.0 ± 0.0	100.0 ± 0.0	97.0 ± 0.8	100.0 ± 0.0

[a]Radiolabeling efficiency (mean ± standard deviation%) was measured in duplicate using TLC (mobile phase: 100 mM EDTA, pH 7.0).

Table 3. Stability of ^{89}Zr-Labeled Chelators in Human Serum (n = 2−3, pH 7.0, 37 °C)[a]

	^{89}Zr-labeled chelator (%)			
time	[^{89}Zr]Zr-NODHA	[^{89}Zr]Zr-NOTHA	[^{89}Zr]Zr-NODHA-PY	[^{89}Zr]Zr-DFO
1 day	100.0 ± 0.0	100.0 ± 0.0	96.8 ± 5.5	100.0 ± 0.0
2 days	100.0 ± 0.0	98.2 ± 2.0	95.8 ± 3.6	100.0 ± 0.0
3 days	100.0 ± 0.0	100.0 ± 0.0	94.8 ± 4.6	100.0 ± 0.0
7 days	100.0 ± 0.0	95.5 ± 4.1	88.5 ± 3.2	100.0 ± 0.0

[a]Bound ^{89}Zr−chelator (mean ± standard deviation%) was measured in duplicate or triplicate by TLC (mobile phase: 100 mM EDTA, pH 7.0).

optimized Zr(IV)-NODHA are more tightly coordinated to Zr(IV) than the nitrogen atoms (mean distance of Zr-O and Zr-N, 2.063 *vs* 2.580 Å). Three hydroxamate groups in NOTHA are predicted to form a hexacoordinate complex with Zr(IV) (mean distance of Zr-O: 2.095 Å), and the nitrogen atoms in the TACN ring of the optimized Zr(IV)-NOTHA complex loosely bound to Zr(IV) (mean distance of Zr-N: 4.377 Å). The optimized structure of the Zr(IV)-(NODHA-PY) complex indicates that NODHA-PY is not capable of adopting an eight-coordinate geometry around Zr(IV) but forms a less stable heptacoordinate complex with Zr(IV). One of the nitrogen atoms (N_1) in the TACN ring of the optimized Zr(IV)-NODHA-PY complex is not found to form a tight bond with Zr(IV). The addition of the pyridyl group into the macrocyclic backbone in NODHA is predicted to generate a considerable ligand strain on the Zr-coordination sphere and results in weaker binding of NODHA-PY to Zr as indicated by a longer bond length of Zr-O (2.114 Å) and Zr-N (2.709 Å).

Radiolabeling and *In Vitro* Complex Stability. The chelators NODHA, NOTHA, NODHA-PY, and DFO were comparatively evaluated for radiolabeling efficiency with ^{89}Zr. The new chelator in 0.25 M NH_4OAc buffer solution (pH 7.0) was radiolabeled with ^{89}Zr at room temperature (RT). During the reaction time (30 min), the radiolabeling kinetics was assessed by TLC analysis (Table 2 and Supporting Information). The radiolabeling data show that all chelates rapidly bound to ^{89}Zr with more than 90% labeling efficiency at the 1 min time point. DFO instantly and completely bound to ^{89}Zr at the 1 min time point. NODHA and NOTHA were more efficient in binding ^{89}Zr than NODHA-PY. Radiolabeling of NODHA or NOTHA with ^{89}Zr was completed at the 30 min time point, while NODHA-PY had a lower labeling

https://doi.org/10.1021/acsomega.2c03478
ACS Omega 2022, 7, 37229−37236

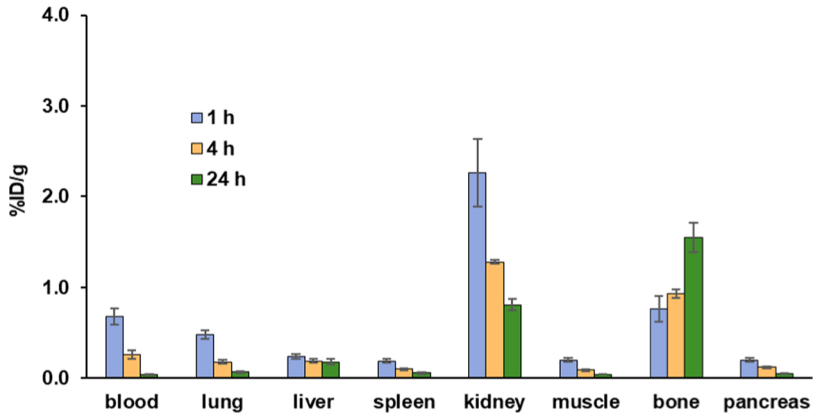

Figure 1. *In vivo* biodistribution of [^{89}Zr]Zr-NODHA in CD-1 mice (n = 4−5, IV injection).

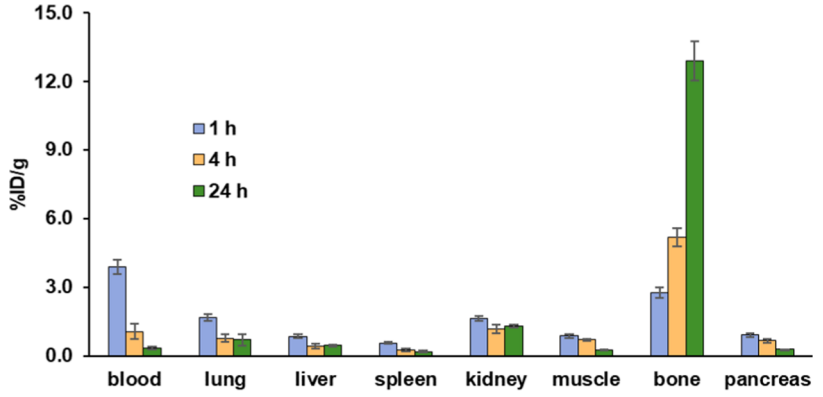

Figure 2. *In vivo* biodistribution of [^{89}Zr]Zr-NODHA-PY in CD-1 mice (n = 4, IV injection).

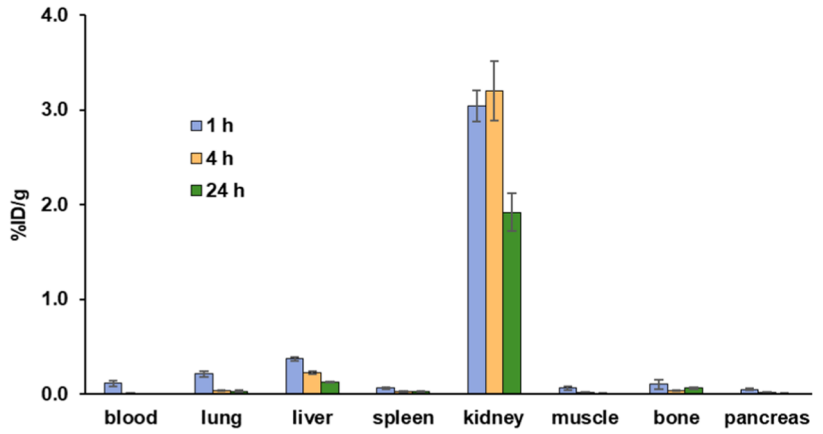

Figure 3. *In vivo* biodistribution of [^{89}Zr]Zr-DFO in CD-1 mice (n = 4, IV injection).

efficiency with ^{89}Zr (97% labeling efficiency at the 30 min time point).

[^{89}Zr]Zr-labeled chelators were further evaluated for complex stability in human serum (Table 3 and Supporting Information). [^{89}Zr]Zr-DFO and [^{89}Zr]Zr-NODHA were stable in human serum for at least 7 days, while a small amount of ^{89}Zr (∼5%) was lost from [^{89}Zr]Zr-NOTHA over 7 days. [^{89}Zr]Zr-NODHA-PY remained unstable in human serum and released a considerable amount of ^{89}Zr (<12%) in human serum over 7 days. The radiolabeling and *in vitro* complex stability data indicate that the heptadentate chelator NODHA displayed excellent radiolabeling kinetics and stability with ^{89}Zr. NOTHA and NODHA-PY were less effective in holding ^{89}Zr than NODHA, and the corresponding [^{89}Zr]Zr-NOTHA and [^{89}Zr]Zr-NODHA-PY complexes have lower stability in human serum than [^{89}Zr]Zr-NODHA.

***In Vivo* Biodistribution.** The comparative *in vivo* stability of [^{89}Zr]Zr-NODHA, [^{89}Zr]Zr-NODHA-PY, and [^{89}Zr]Zr-DFO was evaluated by performing biodistribution studies in CD-1 normal mice (intravenous injection, n = 4−5, Figures 1−3 and Supporting Information). As expected from serum stability data, three chelators labeled with ^{89}Zr produced different *in vivo* biodistribution profiles. [^{89}Zr]Zr-NODHA displayed rapid blood clearance with minimal radioactivity in the blood at all time points (≤0.68% ID/g). [^{89}Zr]Zr-NODHA had a negligible accumulation in the lung, liver, spleen, muscle,

https://doi.org/10.1021/acsomega.2c03478
ACS Omega 2022, 7, 37229−37236

and pancreas at all time points (≤0.48% ID/g), and the radioactivity in the normal organs decreased from 1 to 24 h time point. [^{89}Zr]Zr-NODHA exhibited the highest renal uptake at 1 h (2.26% ID/g), which decreased to a minimal level at the 24 h time point (0.81% ID/g). A considerable activity (1.55% ID/g) of [^{89}Zr]Zr-NODHA was retained in the bones at the 24 h time point. [^{89}Zr]Zr-NODHA had significantly less uptake ($p < 0.05$) than [^{89}Zr]Zr-NODHA-PY in all organs at all time points except for the blood, liver, and spleen at 4 h as well as the kidney at 1 and 4 h, in which the differences were not significant. [^{89}Zr]Zr-NODHA-PY showed poor stability in mice as evidenced by significantly greater ($p < 0.05$) bone accumulation at all time points when compared to [^{89}Zr]Zr-NODHA or [^{89}Zr]Zr-DFO. [^{89}Zr]Zr-NODHA-PY had measurable uptake in the kidneys at all time points (<1.64% ID/g). [^{89}Zr]Zr-NODHA-PY displayed minimal radioactivity in the liver, spleen, muscle, and pancreas at all time points (≤0.90% ID/g). [^{89}Zr]Zr-NODHA-PY had higher activity in the lung at the 1 h time point (1.67% ID/g), which decreased to 0.69% ID/g at the 24 h time point. [^{89}Zr]Zr-NODHA-PY was significantly greater ($p < 0.05$) than [^{89}Zr]Zr-DFO in all organs at all time points except for the blood and liver at 4 h and the kidney, where [^{89}Zr]Zr-DFO was significantly greater at all time points. [^{89}Zr]Zr-DFO had a negligible activity in the blood, lung, liver, spleen, muscle, bone, and pancreas at 24 h postinjection (<0.12% ID/g). [^{89}Zr]Zr-DFO displayed higher radioactivity in the kidneys at all time points when compared to [^{89}Zr]Zr-NODHA and [^{89}Zr]Zr-NODHA-PY. Among the [^{89}Zr]Zr-labeled chelators evaluated, [^{89}Zr]Zr-DFO had the lowest bone uptake at all time points (<0.1% ID/g). [^{89}Zr]Zr-NODHA exhibited better renal clearance than [^{89}Zr]Zr-DFO, while rapid liver clearance was observed for both [^{89}Zr]Zr-NODHA and [^{89}Zr]Zr-DFO.

CONCLUSIONS

We have synthesized and evaluated the novel chelators NODHA, NOTHA, and NODHA-PY for complexation with ^{89}Zr(IV). We have shown that all chelates rapidly bound to ^{89}Zr at room temperature and displayed comparable radiolabeling kinetics to that of DFO. Among the new chelators evaluated, NODHA labeled with ^{89}Zr exhibited excellent complex stability in human serum. [^{89}Zr]Zr-NOTHA and [^{89}Zr]Zr-NODHA-PY remained less stable in human serum and released a considerable amount of ^{89}Zr in human serum. The results of DFT calculations suggest that the chelator NODHA bound to Zr(IV) more tightly than NOTHA and NOTHA-PY. Poor complex stability of [^{89}Zr]Zr-NODHA-PY was further confirmed by high accumulation in the bones of mice. [^{89}Zr]Zr-NODHA had better renal clearance than [^{89}Zr]Zr−DFO, while [^{89}Zr]Zr-NODHA exhibited higher bone uptake than [^{89}Zr]Zr-DFO at all time points. Among the new [^{89}Zr]Zr−chelator complexes studied, [^{89}Zr]Zr-NODHA produced the best serum stability and biodistribution profiles. The *in vitro* and *in vivo* data suggest that NODHA deserves further derivatization for conjugation to an antibody for targeted PET imaging applications.

EXPERIMENTAL SECTION

Instruments and Methods. ^{1}H and ^{13}C NMR spectra were obtained using a Bruker 300 instrument, and chemical shifts are reported in ppm on the δ scale relative to TMS, TSP, or solvent. Electrospray iodization (ESI) high-resolution mass spectra (HRMS) were obtained on a JEOL double-sector JMS-AX505HA mass spectrometer (University of Notre Dame, IN). Analytical HPLC was performed on an Agilent 1200, equipped with a diode array detector, a thermostat set at 35 °C, and a Zorbax Eclipse XDB-C18 column (4.6 mm × 150 mm, 80 Å). The mobile phase of a binary gradient (0−100% B/15 min; solvent A, 0.1% TFA in H_2O; solvent B, 0.1% TFA in CH_3CN for method 1) at a flow rate of 1 mL/min was used. Semipreparative HPLC was performed on an Agilent 1200, equipped with a diode array detector, a thermostat set at 35 °C, and a Zorbax Eclipse XDB-C18 column (9.4 mm × 250 mm, 80 Å). The mobile phase of a binary gradient (0−100% B/25 min; solvent A = 0.1% TFA in water; solvent B = 0.1% TFA in acetonitrile for method 2) at a flow rate of 3 mL/min was used for semiprep HPLC. All reagents were purchased from Sigma-Aldrich or Acros Organics and used as received unless otherwise noted.

*N-[(4-Methoxyphenyl)methoxy]-2-[4-({[(4-methoxyphenyl)methoxy](methyl)carbamoyl} methyl)-1,4,7-triazonan-1-yl]-N-methylacetamide (**3**) and 2-[4,7-Bis({[(4-methoxyphenyl)methoxy](methyl)carbamoyl}-methyl)-1,4,7-triazonan-1-yl]-N-[(4-methoxyphenyl)-methoxy]-N-methylacetamide (**4**).* To a solution of TACN **1** (50.0 mg, 0.39 mmol) in CH_2Cl_2 (5 mL) was added compound **2**[18] (245.3 mg, 0.85 mmol) in CH_2Cl_2 (3 mL) at 0 °C. The resulting mixture was stirred for 6 days at room temperature and concentrated to dryness *in vacuo* and purified by semiprep HPLC (method 2) to afford compound **3** (72.5 mg, 34.4%) and compound **4** (21 mg, 15.5%).

Compound **3**. Analytical HPLC (t_R = 9.74 min, method 1). ^{1}H NMR ($CDCl_3$, 300 MHz) δ 2.69−2.72 (m, 4H), 2.90−3.00 (m, 4H), 3.12−3.19 (m, 4H), 3.21 (s, 6H), 3.43 (s, 4H), 3.81 (s, 6H), 4.75 (s, 4H), 6.92 (d, J = 8.4 Hz, 4H), 7.30 (d, J = 8.6 Hz, 4H). ^{13}C NMR ($CDCl_3$, 75 MHz) δ 33.3 (q), 44.0 (t), 50.9 (t), 52.3 (t), 55.3 (q), 56.2 (t), 75.6 (t), 114.2 (d), 125.8 (s), 131.5 (d), 160.5 (s), 170.4 (s). HRMS (ESI) calcd for $C_{28}H_{42}N_5O_6$ $[M + H]^+$ m/z 544.3130. Found: $[M + H]^+$ m/z 544.3148.

Compound **4**. Analytical HPLC (t_R = 11.92 min, method 1). ^{1}H NMR ($CDCl_3$, 300 MHz) δ 2.96 (s, 12H), 3.20 (s, 9H), 3.74−3.79 (m, 15H), 4.78 (s, 6H), 6.90 (d, J = 8.5 Hz, 6H), 7.33 (d, J = 8.5 Hz, 6H). ^{13}C NMR ($CDCl_3$, 75 MHz) δ 33.4 (q), 51.0 (t), 55.3 (q), 55.8 (t), 75.6 (t), 114.2 (d), 126.0 (s), 131.5 (d), 160.5 (s), 169.4 (s). HRMS (ESI) calcd for $C_{39}H_{55}N_6O_9$ $[M + H]^+$ m/z 751.4025. Found: $[M + H]^+$ m/z 751.4050.

*N-Hydroxy-2-(4-{[hydroxy(methyl)carbamoyl]methyl}-1,4,7-triazonan-1-yl)-N-methylacetamide (**5**).* To compound **3** (12.0 mg, 0.02 mmol) was added TFA (1 mL) and triethylsilane (10.3 mg, 0.09 mmol) at 0 °C. The resulting mixture was stirred for 14 h at room temperature. The reaction mixture was concentrated to dryness *in vacuo* and washed with CH_2Cl_2 to afford compound **5** (5.4 mg, 81%). Analytical HPLC (t_R = 2.85 min, method 1). ^{1}H NMR (D_2O, 300 MHz) δ 3.14 (s, 6H), 3.18−3.22 (m, 4H), 3.30−3.44 (m, 8H), 4.06 (s, 4H). ^{13}C NMR (D_2O, 75 MHz) δ 36.2 (q), 43.1 (t), 50.4 (t), 51.5 (t), 56.2 (t), 169.5 (s). HRMS (ESI) calcd for $C_{12}H_{26}N_5O_4$ $[M + H]^+$ m/z 304.1979. Found: $[M + H]^+$ m/z 304.1981.

*2-(4,7-di{[Hydroxy(methyl)carbamoyl]methyl}-1,4,7-triazonan-1-yl)-N-hydroxy-N-methylacetamide (**6**).* To compound **4** (12.0 mg, 0.02 mmol) was added TFA (1 mL) and triethylsilane (11.6 mg, 0.10 mmol) at 0 °C. The resulting

https://doi.org/10.1021/acsomega.2c03478
ACS Omega 2022, 7, 37229−37236

mixture was stirred for 14 h at room temperature. The reaction mixture was concentrated to dryness *in vacuo* and washed with CH_2Cl_2 to afford compound **6** (6.0 mg, 93%). Analytical HPLC (t_R = 5.38 min, method 1). ^{1}H NMR (D_2O, 300 MHz) δ 3.14 (s, 9H), 3.45 (s, 12H), 4.21 (s, 6H). ^{13}C NMR (D_2O, 75 MHz) δ 36.2 (q), 51.2 (t), 56.4 (t), 168.3 (s). HRMS (ESI) calcd for $C_{15}H_{30}N_6O_6$ $[M + H]^+$ m/z 391.2300. Found: $[M + H]^+$ m/z 391.2285.

*tert-Butyl 1,4,7-triazonane-1-carboxylate (**7**).*[20] To a solution of 1,4,7-triazacyclononane (200.3 mg, 1.55 mmol) in CH_2Cl_2 (50 mL) at −5 °C was added dropwise *tert*-butyl[(*E*)-[cyano(phenyl)methylidene]amino] carbonate (BOC-ON) (362.0 mg, 1.47 mmol) in CH_2Cl_2 (35 mL) over 1 h. After addition was completed, the reaction mixture was concentrated *in vacuo*. The residue was treated with 1 M NaOH (30 mL), and the resulting solution was extracted with diethyl ether (2 × 30 mL) and dichloromethane (2 × 30 mL). The organic layers containing the product were combined and dried over $MgSO_4$, filtered, and concentrated *in vacuo* to afford compound **7** (74 mg, 21.8%). ^{1}H NMR ($CDCl_3$, 300 MHz) δ 1.45 (s, 9H), 2.40 (s, 2H), 2.72 (s, 4H), 2.91−2.96 (m, 4H), 3.27−3.34 (m, 4H). ^{13}C NMR ($CDCl_3$, 75 MHz) δ 28.5 (q), 47.2 (t), 48.1 (t), 48.9 (t), 54.3 (t), 54.6 (t), 79.5 (s), 155.5 (s). HRMS (ESI) calcd for $C_{11}H_{24}N_3O_2$ $[M + H]^+$ m/z 230.1863. Found: $[M + H]^+$ m/z 230.1852.

*tert-Butyl 4,7-bis({[(4-methoxyphenyl)methoxy](methyl)-carbamoyl}methyl)-1,4,7-triazonane-1-carboxylate (**8**).* To a solution of compound **7** (50.0 mg, 0.218 mmol) in CH_3CN (1 mL) was added K_2CO_3 and compound **2** (125.6 mg, 0.436 mmol) in CH_3CN at 0 °C. The resulting mixture was stirred for 16 h at room temperature. The reaction mixture was filtered while washing with CH_2Cl_2 and concentrated to dryness *in vacuo*. The residue was purified *via* column chromatography on silica gel (60−220 mesh) eluting with 3−5% CH_3OH in CH_2Cl_2 to afford **8** (118.1 mg, 84.4%). ^{1}H NMR ($CDCl_3$, 300 MHz) δ 1.45 (s, 9H), 2.72−3.49 (m, 22H), 3.81 (s, 6H), 4.77 (s, 4H), 6.91 (d, J = 8.1 Hz, 4H), 7.33−7.36 (m, 4H). ^{13}C NMR ($CDCl_3$, 75 MHz) δ 28.5 (q), 29.7 (t), 33.5 (q), 49.5 (t), 50.2 (t), 53.4 (t), 55.3 (q), 56.8 (t), 75.8 (t), 79.2 (s), 114.1 (d), 126.4 (s), 131.3 (d), 155.5 (s), 160.3 (s), 173.5 (s). HRMS (ESI) calcd for $C_{33}H_{50}N_5O_8$ $[M + H]^+$ m/z 644.3654. Found: $[M + H]^+$ m/z 644.3647.

*N-[(4-Methoxyphenyl)methoxy]-2-[4-({[(4-methoxyphenyl)methoxy](methyl)carbamoyl} methyl)-1,4,7-triazonan-1-yl]-N-methylacetamide (**3**).* To a solution of **8** (20.3 mg, 0.032 mmol) in CH_2Cl_2 (1 mL) was added TFA (1 mL) at 0 °C. The resulting mixture was stirred for 1 h at room temperature. The reaction mixture was concentrated *in vacuo* and washed with diethyl ether several times to afford compound **3** (16.4 mg, 95.9%). ^{1}H NMR ($CDCl_3$, 300 MHz) δ 2.69−2.72 (m, 4H), 2.90−3.00 (m, 4H), 3.12−3.19 (m, 4H), 3.21 (s, 6H), 3.43 (s, 4H), 3.81 (s, 6H), 4.75 (s, 4H), 6.92 (d, J = 8.4 Hz, 4H), 7.30 (d, J = 8.6 Hz, 4H). ^{13}C NMR ($CDCl_3$, 75 MHz) δ 33.3 (q), 44.0 (t), 50.9 (t), 52.3 (t), 55.3 (q), 56.2 (t), 75.6 (t).114.2 (d), 125.8 (s), 131.5 (d), 160.5 (s), 170.4 (s). ^{1}H and ^{13}C NMR spectra data of **3** obtained from this reaction are the same as those of **3** obtained from the reaction described above.

*N-[(4-Methoxyphenyl)methoxy]-2-[4-({[(4-methoxyphenyl)methoxy](methyl)carbamoyl} methyl)-7-[(pyridin-2-yl)methyl]-1,4,7-triazonan-1-yl]-N-methylacetamide (**9**).* To a solution of **3** (46.6 mg, 0.086 mmol) in CH_2Cl_2 (5 mL) was added 2-formyl pyridine (20.2 mg, 0.188 mmol) at room temperature. The resulting mixture was stirred for 40 min and treated with $NaBH(OAc)_3$ (72.0 mg, 0.340 mmol) and continuously stirred for 24 h and concentrated *in vacuo*. The residue was purified by semiprep HPLC (method 2) to afford compound **9** (20.0 mg, 36.6%). Analytical HPLC (t_R = 9.80 min, method 1). ^{1}H NMR ($CDCl_3$, 300 MHz) δ 2.85−2.94 (m, 4H), 2.97−3.11 (m, 8H), 3.22 (s, 6H), 3.75 (s, 4H), 3.80 (s, 6H), 4.30 (s, 2H), 4.78 (s, 4H), 6.89 (d, J = 8.4 Hz, 4H), 7.30 (d, J = 8.5 Hz, 4H), 7.74 (t, J = 6.4 Hz 1H), 7.99 (d, J = 7.3 Hz, 1H), 8.23 (t, J = 7.2 Hz, 1H), 8.75 (d, J = 5.2 Hz, 1H). ^{13}C NMR ($CDCl_3$, 75 MHz) δ 33.4 (q), 49.4 (t), 50.5 (t), 51.8 (t), 55.3 (q), 55.6 (t), 57.3 (t), 75.8 (t), 114.2 (d), 125.5 (d), 125.9 (d), 127.3 (s), 131.4 (d), 143.3 (d), 144.3 (d), 153.3 (s), 160.5 (s), 169.4 (s). HRMS (ESI) calcd for $C_{34}H_{47}N_6O_6$ $[M + H]^+$ m/z 635.3552. Found: $[M + H]^+$ m/z 635.3559.

*N-Hydroxy-2-(4-{[hydroxy(methyl)carbamoyl]methyl}-7-[(pyridin-2-yl)methyl]-1,4,7-triazonan-1-yl)-N-methylacetamide (**10**).* To a solution of **9** (17 mg, 0.027 mmol) in CH_2Cl_2 (2 mL) was added trifluoroacetic acid (1 mL) and triethylsilane (6.38 mg, 0.054 mmol) at 0 °C. The resulting mixture was stirred for 6 h at room temperature and concentrated *in vacuo*. The residue was washed with ether (3 × 10 mL) and purified by semiprep HPLC (method 2) to afford compound **10** (3.4 mg, 31.9%). Analytical HPLC (t_R = 5.88 min, method 1). ^{1}H NMR (D_2O, 300 MHz) δ 2.53−3.16 (m, 18H), 3.94−4.22 (m, 6H), 7.86 (t, J = 6.6 Hz, 1H), 7.98 (d, J = 8.2 Hz, 1H), 8.43 (t, J = 7.6 Hz, 1H), 8.52 (d, J = 6.4 Hz, 1H). ^{13}C NMR (D_2O, 75 MHz) δ 36.1 (q), 47.8 (t), 49.5 (t), 51.0 (t), 54.3 (t), 56.6 (t), 126.4 (d), 127.9 (d), 141.4 (d), 147.3 (d), 153.2 (s), 169.1 (s). HRMS (ESI) calcd for $C_{18}H_{30}N_6O_4$ $[M + H]^+$ m/z 395.2401. Found: $[M + H]^+$ m/z 395.2394.

Computational Studies. Geometries of Zr(IV) complexes were optimized using a highly efficient electronic structure approach, PBEh-3c.[21] A hybrid Perdew−Burke−Ernzerhof (PBE) functional with 42% of nonlocal Fock exchange was employed. All atoms were described using the basis set of double-ζ quality, def2-mSVP,[21] which includes the effective core potential (ECP) developed by Stuttgart and Dresden for Zr.[22] Basis set superposition errors (BSSEs) and London dispersion effects were accounted by the implementation of geometrical counterpart (gCP)[23] and dispersion correction (D3)[24] schemes, respectively. To accelerate calculations, the "resolution-of-identity" (RI)[25] approximation to Coulomb term and the corresponding auxiliary basis set[26] for Coulomb fitting were utilized. All calculations were performed using the ORCA 4.0.0 program.[27]

Radiolabeling of Chelating Agents with ^{89}Zr. An ultrapure HCl solution (JT Baker, #6900−05) was used to prepare all HCl solutions. Plasticware including pipette tips, tubes, and caps were soaked in 0.1 M HCl overnight and washed thoroughly with Milli-Q (18.2 MΩ) water and air-dried overnight. Ultrapure ammonium acetate (Aldrich, #372331) was used to prepare 0.25 M NH_4OAc buffer solution (0.25 M, pH 7.0). After being adjusted to pH 7.0 using 0.1 M, 1 M HCl, or NaOH solution, a 0.25 M NH_4OAc buffer solution was treated with Chelex-100 resin (Bio-Rad lab, #142-2842), shaken overnight at room temperature, and filtered through a 0.22 μM filter (Corning, #430320) prior to use. TLC plates (2 cm × 6.6 cm, silica gel 60 F_{254}, EMD Chemicals Inc., #5554-7) with the origin line drawn at 0.6 cm from the bottom of TLC were prepared. A stock solution of

https://doi.org/10.1021/acsomega.2c03478
ACS Omega 2022, 7, 37229−37236

^{89}Zr (75 μL, 3 mCi) was adjusted to pH 7.0 by adding 1 M Na_2CO_3 solution that was chelexed.

A buffer solution (0.25 M NH_4OAc, pH 7.0), chelator (25 nmol) with a concentration of 10 mM dissolved in buffer solution, and ^{89}Zr (0.74 MBq, 20 μCi) were sequentially added to a microcentrifuge tube (1.5 mL). The total volume of the reaction mixture was 10 μL. The resulting mixture was agitated at room temperature for 30 min using a thermomixer (Eppendorf, 5355) set at 1000 rpm. Labeling efficiency of the complexes was determined by TLC using a TLC scanner (Bioscan, B-FC-100). The reaction mixture (2.0 μL) withdrawn at each designated time point was spotted on the TLC plate and eluted with the mobile phase (100 mM EDTA, pH 7.0). After elution was completed, the TLC plate was dried on the surface of a heating plate set at 35 °C. Bound and unbound ^{89}Zr appeared 30−45 and 50−60 mm from the bottom line of TLC, respectively.

Serum Stability of [^{89}Zr]Zr−Chelators. Human serum was purchased from Gemini Bioproducts (#100110). A [^{89}Zr]Zr-labeled chelator was freshly prepared by the reaction of a chelator (0.075 μmol) with ^{89}Zr (2.22 MBq, 60 μCi) in 0.25 M NH_4OAc buffer (pH 7.0) for 1 h at room temperature. The total volume of the reaction mixture was 20 μL. Labeling efficiency of the [^{89}Zr]Zr-labeled complex was determined to be 100% by TLC analysis. Therefore, the freshly prepared [^{89}Zr]Zr-labeled complex was directly used for serum stability studies without purification. Human serum (80 μL) was added to a solution of the [^{89}Zr]Zr-labeled chelator (60 μCi) in a microcentrifuge tube. The [^{89}Zr]Zr-labeled chelator in human serum was incubated at 37 °C for 7 days. Stability of the [^{89}Zr]Zr-labeled chelator in human serum was determined by TLC (eluent: 100 mM EDTA, pH = 7.0). Bound and unbound ^{89}Zr appeared 30−45 and 50−60 mm from the bottom line of TLC, respectively.

***In Vivo* Biodistribution.** All solvents and reagents were ultrapure or trace metal grade and obtained from Sigma-Aldrich (St. Louis, MO) and used as received unless stated otherwise. All solutions and buffers were prepared using water purified from a Millipore Integral 5 Milli-Q water system (18 MΩ·cm resistivity, Billerica, MA). All buffers were treated with Chelex overnight and filtered through a 0.22 μm nylon filter to remove trace amounts of metal ions. Radioactivity was counted with a Beckman γ 8000 counter containing a NaI crystal (Beckman Instruments, Inc., Irvine, CA). ^{89}Zr was produced via the ^{89}Y(p,n)^{89}Zr reaction on a TR-19 biomedical cyclotron (Advanced Cyclotron Systems Inc., Richmond, BC, Canada) at the Department of Radiology, Washington University School of Medicine.[13] Dissolution of the target and the separation steps were conducted through an automated module to reduce operator exposure. About 37 MBq (1 mCi) of ^{89}Zr-oxalate solution (pH ≤ 1) was neutralized to pH 7.1−7.4 by first adding an equivalent volume of 0.25 M NH_4OAc (pH 7.0), followed by slow addition of 2 M NaOH. Each chelator was radiolabeled by adding 50 μg of chelator to 3.7 MBq (100 μCi) of neutralized [^{89}Zr]Zr-oxalate in 30 μL of 0.25 M NH_4OAc (pH 7.0). The reactions were incubated on a thermomixer with 1000 rpm agitation at room temperature for 1 h. Radiochemical purity was determined by TLC with a mobile phase of 100 mM EDTA (pH 7.0). A radiochemical yield of greater than 99% was achieved and therefore used without further purification.

The animal experiment was performed in compliance with the Guidelines for Care and Use of Research Animals established by the Division of Comparative Medicine and the Animal Studies Committee of Washington University School of Medicine. Biodistribution studies were conducted in female 5−7 week old CD-1 mice (Charles River Laboratories). Animals were injected with ∼0.19 MBq (∼5 μCi, 100 μL of PBS) of [^{89}Zr]Zr-NODHA, [^{89}Zr]Zr-NODHA-PY, or [^{89}Zr]Zr-DFO while being anesthetized with 2% isoflurane. Pancreas, liver, kidney, and other organs of interest were harvested at 1, 4, and 24 h postinjection. The amount of radioactivity in each organ was determined by γ counting and the percent injected dose per gram of tissue (%ID/g) calculated. Samples were calibrated against a known standard. Quantitative data were processed by Prism 7 (GraphPad Software, v 7.00, La Jolla, CA) and expressed as mean ± SEM. Statistical analysis was performed using an unpaired *t*-test with Welch's correction. Differences at the 95% confidence level ($p < 0.05$) were considered statistically significant (Table 3).

■ ASSOCIATED CONTENT

Supporting Information

The Supporting Information is available free of charge at https://pubs.acs.org/doi/10.1021/acsomega.2c03478.

Copies of NMR spectra and copies of TLC chromatograms for assessment of radiolabeling reaction kinetics and serum stability and *in vivo* biodistribution data (PDF)

■ AUTHOR INFORMATION

Corresponding Author

Hyun-Soon Chong − *Department of Chemistry, Illinois Institute of Technology, Chicago, Illinois 60616, United States;* orcid.org/0000-0003-0299-7601; Email: Chong@iit.edu; Fax: 312-567-3494

Authors

Chi Soo Kang − *Department of Chemistry, Illinois Institute of Technology, Chicago, Illinois 60616, United States*

Shuyuan Zhang − *Department of Chemistry, Illinois Institute of Technology, Chicago, Illinois 60616, United States*

Haixing Wang − *Department of Chemistry, Illinois Institute of Technology, Chicago, Illinois 60616, United States*

Yujie Liu − *Department of Chemistry, Illinois Institute of Technology, Chicago, Illinois 60616, United States*

Siyuan Ren − *Department of Chemistry, Illinois Institute of Technology, Chicago, Illinois 60616, United States*

Yanda Chen − *Department of Chemistry, Illinois Institute of Technology, Chicago, Illinois 60616, United States*

Jingbai Li − *Department of Chemistry, Illinois Institute of Technology, Chicago, Illinois 60616, United States;* orcid.org/0000-0003-4743-0318

Nilantha Bandara − *Department of Radiation Oncology, Washington University School of Medicine, St. Louis, Missouri 63100-1010, United States*

Andrey Yu Rogachev − *Department of Chemistry, Illinois Institute of Technology, Chicago, Illinois 60616, United States;* orcid.org/0000-0001-9855-7824

Buck E. Rogers − *Department of Radiation Oncology, Washington University School of Medicine, St. Louis, Missouri 63100-1010, United States;* orcid.org/0000-0001-8189-1797

https://doi.org/10.1021/acsomega.2c03478
ACS Omega 2022, 7, 37229−37236

Complete contact information is available at:
https://pubs.acs.org/10.1021/acsomega.2c03478

Notes

The authors declare no competing financial interest.

■ ACKNOWLEDGMENTS

This research was partly supported by the National Institutes of Health (R01CA112503 and R01EB029800 to H.-S.C.). The authors would like to thank the small animal imaging facility at Washington University School of Medicine for excellent technical assistance in conducting biodistribution studies. They would also like to acknowledge the Isotope Production Group at Washington University for production of ^{89}Zr.

■ REFERENCES

(1) Gambhir, S. S. Molecule imaging of cancer with positron emission tomography. *Nat. Rev. Cancer* **2002**, *2*, 683−693.
(2) Juweid, M. E.; Cheson, B. D. Positron-emission tomography and assessment of cancer therapy. *N. Engl. J. Med.* **2006**, *354*, 496−507.
(3) Phelps, M. E. Positron emission tomography provides molecular imaging of biological processes. *Proc. Natl. Acad. Sci.* **2000**, *97*, 9226−9233.
(4) Fletcher, J. W.; Djulbegovic, B.; Soares, H. P.; Siegel, B. A.; Lowe, V. J.; Lyman, G. H.; Coleman, R. E.; Wahl, R.; Paschold, J. C.; Avril, N.; Einhorn, L. H.; Suh, W. W.; Samson, D.; Delbeke, D.; Gorman, M.; Shields, A. F. Recommendations on the use of ^{18}F-FDG PET in oncology. *J. Nucl. Med.* **2008**, *49*, 480−508.
(5) Lee, F. T.; Scott, A. M. Immuno-PET for tumor targeting. *J. Nucl. Med.* **2003**, *44*, 1282−1283.
(6) Wei, W.; Rosenkrans, Z. T.; Liu, J.; Huang, G.; Luo, Q-Y.; Cai, W. ImmunoPET: Concept, Design, and Applications. *Chem. Rev.* **2020**, *120*, 3787−3851.
(7) Heskamp, S.; Raavé, R.; Boerman, O.; Rijpkema, M.; Goncalves, V.; Denat, F. ^{89}Zr-immuno-positron emission tomography in oncology: state-of-the-art ^{89}Zr radiochemistry. *Bioconjugate Chem.* **2017**, *28*, 2211−2223.
(8) Wadas, T. J.; Wong, E. H.; Weisman, G. R.; Anderson, C. J. Coordinating radiometals of copper, gallium, indium, yttrium, and zirconium for PET and SPECT imaging of disease. *Chem. Rev.* **2010**, *110*, 2858−2902.
(9) Nayak, T. K.; Brechbiel, M. W. Radioimmunoimaging with longer-lived positron-emitting radionuclides: Potentials and challenges. *Bioconjugate Chem.* **2009**, *20*, 825−841.
(10) Deri, M. A.; Zeglis, B. M.; Francesconi, L. C.; Lewis, J. S. PET Imaging with ^{89}Zr: From Radiochemistry to the Clinic. *Nucl. Med. Biol.* **2013**, *40*, 3−14.
(11) Severin, G. W.; Engle, J. W.; Nickles, R. J.; Barnhart, T. E. ^{89}Zr Radiochemistry for PET. *Med. Chem.* **2011**, *7*, 389−394.
(12) Holland, J. P.; Sheh, Y.; Lewis, J. S. Standardized methods for the production of high specific-activity zirconium-89. *Nucl. Med. Biol.* **2009**, *36*, 729−739.
(13) (a) Bhatt, N. B.; Pandya, D. N.; Wadas, T. J. Recent advances in zirconium-89 chelator development. *Molecules* **2018**, *23*, No. 638. (b) Boros, E.; Holland, J. P.; Kenton, N.; Rotile, N.; Caravan, P. Macrocycle-Based Hydroxamate Ligands for Complexation and Immunoconjugation of ^{89}Zirconium for Positron Emission Tomography (PET) Imaging. *ChemPlusChem* **2016**, *81*, 274−281. (c) Pandya, D. N.; Henry, K. E.; Day, C. S.; Graves, S. A.; Nagle, V. L.; Dilling, T. R.; Sinha, A.; Ehrmann, B. M.; Bhatt, N. B.; Menda, Y.; Lewis, J. S.; Wadas, T. J. Polyazamacrocycle Ligands Facilitate ^{89}Zr Radiochemistry and Yield ^{89}Zr Complexes with Remarkable Stability. *Inorg. Chem.* **2020**, *59*, 17473−17487. (d) Raavé, R.; Sandker, G.; Adumeau, P.; Jacobsen, C. B.; Mangin, F.; Meyer, M.; Moreau, M.; Bernhard, C.; Da Costa, L.; Dubois, A.; Goncalves, V.; Gustafsson, M.; Rijpkema, M.; Boerman, O.; Chambron, J-C.; Heskamp, S.; Denat, F. Direct comparison of the in vitro and in vivo stability of DFO, DFO* and DFOcyclo* for ^{89}Zr-immunoPET. *Eur. J. Nucl. Med. Mol. Imaging* **2019**, *46*, 1966−1977. (e) Seibold, U.; Wängler, B.; Wängler, C. Rational design, development, and stability assessment of a macrocyclic four-hydroxamate-bearing bifunctional chelating agent for ^{89}Zr. *ChemMedChem* **2017**, *12*, 1555−1571. (f) Deri, M. A.; Ponnala, S.; Zeglis, B. M.; Pohl, G.; Dannenberg, J. J.; Lewis, J. S.; Francesconi, L. C. Alternative chelator for ^{89}Zr radiopharmaceuticals: radiolabeling and evaluation of 3,4,3-(LI-1,2-HOPO). *J. Med. Chem.* **2014**, *57*, 4849−4860. (g) Patra, M.; Bauman, A.; Mari, C.; Fischer, C. A.; Blacque, O.; Häussinger, D.; Gasser, G.; Mindt, T. L. An octadentate bifunctional chelating agent for the development of stable zirconium-89 based molecular imaging probes. *Chem. Commun.* **2014**, *50*, 11523−11525. (h) Guérard, F.; Lee, Y-S.; Brechbiel, M. W. Rational Design, Synthesis, and Evaluation of Tetrahydroxamic Acid Chelators for Stable Complexation of Zirconium(IV). *Chem. - Eur. J.* **2014**, *20*, 5584−5591.
(14) Vosjan, M. J. W. D.; Perk, L. R.; Visser, G. W. M.; Budde, M.; Jurek, P.; Kiefer, G. E.; van Dongen, G. A. M. S. Conjugation and radiolabeling of monoclonal antibodies with zirconium-89 for PET imaging using the bifunctional chelate p-isothiocyanatobenzyl-desferrioxamine. *Nat. Protoc.* **2010**, *5*, 739−743.
(15) Meijs, W. E.; Herscheid, J. D. M.; Haisma, H. J.; Pinedo, H. M. Evaluation of desferal as a bifunctional chelating agent for labeling antibodies with Zr-89. *Int. J. Appl. Radiat. Instrum. Part A. Appl. Radiat. Isot.* **1992**, *43*, 1443−1447.
(16) Fischer, G.; U Seibold, U.; Schirrmacher, R.; Wängler, B.; Wängler, C. ^{89}Zr, a Radiometal Nuclide with High Potential for Molecular Imaging with PET: Chemistry, Applications and Remaining Challenges. *Molecules* **2013**, *18*, 6469−6490.
(17) Abou, D. S.; Ku, T.; Smith-Jones, T. M. In vivo biodistribution and accumulation of ^{89}Zr in mice. *Nucl. Med. Biol.* **2011**, *38*, 675−681.
(18) Zhang, S.; Wang, H.; Ren, S.; Chen, Y.; Liu, D.; Li, M.; Sagastume, E.; Chong, H-S. Synthesis and evaluation of diaza-crown ether-backboned chelator containing hydroxamate groups for Zr-89 chelation chemistry. *Bioorg. Med. Chem. Lett.* **2022**, *72*, No. 128847.
(19) Winchell, H. S.; Klein, J. Y.; Simhon, E. D.; Cyjon, R. L.; Klein, O.; Zaklad, H. Compounds with chelation affinity and selectivity for first transition elements and their use in cosmetics and personal care products, inhibition of metalloenzymes, and inhibition of reperfusion injury. US6,264,966 B1, July 24, 2001.
(20) Kovacs, Z.; Sherry, A. D. A general synthesis of mono- and disubstituted 1,4,7-triazacyclononanes. *Tetrahedron Lett.* **1995**, *36*, 9269−9272.
(21) Grimme, S.; Brandenburg, J. G.; Bannwarth, C.; Hansen, A. Consistent structures and interactions by density functional theory with small atomic orbital basis sets. *J. Chem. Phys.* **2015**, *143*, No. 054107.
(22) Leininger, T.; Nicklass, A.; Kuechle, W.; Stoll, H.; Dolg, M.; Bergner, A. The accuracy of the pseudopotential approximation: non-frozen-core effects for spectroscopic constants of alkali fluorides XF (X = K, Rb, Cs). *Chem. Phys. Lett.* **1996**, *255*, 274−280.
(23) Kruse, H.; Grimme, S. A geometrical correction for the inter- and intra-molecular basis set superposition error in Hartree-Fock and density functional theory calculations for large systems. *J. Chem. Phys.* **2012**, *136*, No. 154101.
(24) (a) Grimme, S.; Ehrlich, S.; Goerigk, L. Effect of the damping function in dispersion corrected density functional theory. *J. Comput. Chem.* **2011**, *32*, 1456−1465. (b) Grimme, S.; Antony, J.; Ehrlich, S.; Krieg, H. A consistent and accurate ab initio parametrization of density functional dispersion correction (DFT-D) for the 94 elements H-Pu. *J. Chem. Phys.* **2010**, *132*, No. 154104.
(25) Kendall, R. A.; Früchtl, H. A. The impact of the resolution of the identity approximate integral method on modern ab initio algorithm development. *Theor. Chem. Acc.* **1997**, *97*, 158−163.
(26) Weigend, F. Accurate Coulomb-fitting basis sets for H to Rn. *Phys. Chem. Chem. Phys.* **2006**, *8*, No. 1057.
(27) Neese, F. The ORCA program system. *Wiley Interdiscip. Rev.: Comput. Mol. Sci.* **2012**, *2*, 73−78.